THE JOURNAL OF PHYSICAL CHEMISTRY B
A JOURNAL OF THE AMERICAN CHEMICAL SOCIETY

pubs.acs.org/JPCB
Article

A Membrane-Assisted Mechanism for the Release of Ceramide from the CERT START Domain

Published as part of The Journal of Physical Chemistry B virtual special issue "Charles L. Brooks III Festschrift".

Mahmoud Moqadam, Parveen Gartan, Reza Talandashti, Antonella Chiapparino, Kevin Titeca, Anne-Claude Gavin, and Nathalie Reuter*

Cite This: J. Phys. Chem. B 2024, 128, 6338–6351

Read Online

ACCESS | Metrics & More | Article Recommendations | Supporting Information

ABSTRACT: Ceramide transfer protein CERT is the mediator of nonvesicular transfer of ceramide from the ER to Golgi. In CERT, START is the domain responsible for the binding and transport of ceramide. A wealth of structural data has revealed a helix-grip fold surrounding a large hydrophobic cavity holding the ceramide. Yet, little is known about the mechanisms by which START releases the ceramide through the polar region and into the packed environment of cellular membranes. As such events do not lend themselves easily to experimental investigations, we used multiple unbiased microsecond-long molecular simulations. We propose a membrane-assisted mechanism in which the membrane acts as an allosteric effector initiating the release of ceramide and where the passage of the ceramide acyl chains is facilitated by the intercalation of a single phosphatidylcholine lipid in the cavity, practically greasing the ceramide way out. We verify using free energy calculation and experimental lipidomics data that CERT forms stable complexes with phosphatidylcholine lipids, in addition to ceramide, thus providing validation for the proposed mechanism.

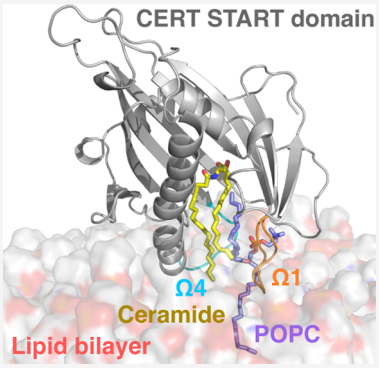

INTRODUCTION

Ceramide (Cer) is the main precursor for the synthesis of signaling and complex sphingolipids present in mammalian membranes. Cer is synthesized in the endoplasmic reticulum (ER) and transported to the trans-Golgi region for further conversion to sphingomyelin for example.[1] The ceramide transfer protein, known as CERT or STARD11, has been identified as the mediator of nonvesicular transfer of Cer from the ER to Golgi at membrane contact sites. CERT consists of two domains linked by a disordered middle region (MR):[2,3] a N-terminal pleckstrin homology (PH) domain[4] associated with the Golgi apparatus and a C-terminal steroidogenic acute regulatory protein (StAR)-related lipid transfer domain, named START in CERT[5] and responsible for the binding and transport of ceramide. The MR contains a serine-repeated motif (SRM) and a diphenylalanine in an acidic tract (FFAT) motif associated with ER-resident membrane proteins (Figure 1A,B). Regulation of CERT activity depends on the phosphorylation in the SRM and FFAT motifs. The former reduces phosphatidylinositol-4-phosphate (PI(4)P) binding and downregulates the activity of CERT, and the latter facilitates the VAP binding of the protein, leading to an enhanced transport of ceramide to the Golgi.[6] In addition, the isolated START and PH domains physically interact, suggesting the existence of an intramolecular regulation mechanism.[6] While all the domains and motifs are required for the full activity of CERT, the START domain alone showed substantial activity for ceramide extraction and transport.[7] Deletion of the START domain completely revoked the transfer activity, whereas mutants in which the PH or MR domains were deleted retained this activity. The START domain is thought to bind the donor membrane via binding loops, to take up a ceramide into a hydrophobic lipid-binding cavity, and to transfer it to the acceptor membrane.[5]

CERT belongs to the StART family of the StARkin superfamily, which is the largest group of lipid transfer proteins (LTPs). LTPs cover a variety of folds that have as a common trait a hydrophobic lipid-binding cavity shielding their cargo from the aqueous environment.[8,9] The structure of proteins in the StARkin superfamily, which also includes phosphatidylinositol transfer proteins (PITPs),[10,11] proline-rich EVH1 ligand 1 (PRELI), and the yeast unprocessed (Ups)[12−14] proteins, consists of an arrangement of a β-sheet and helices forming the hydrophobic cavity. Access to the hydrophobic cavity is thought to be controlled by at least one loop acting as a gate, but the molecular mechanism involved has not been elucidated. In the CERT START domain, this

Received: April 12, 2024
Revised: May 26, 2024
Accepted: June 11, 2024
Published: June 21, 2024

https://doi.org/10.1021/acs.jpcb.4c02398
J. Phys. Chem. B 2024, 128, 6338−6351

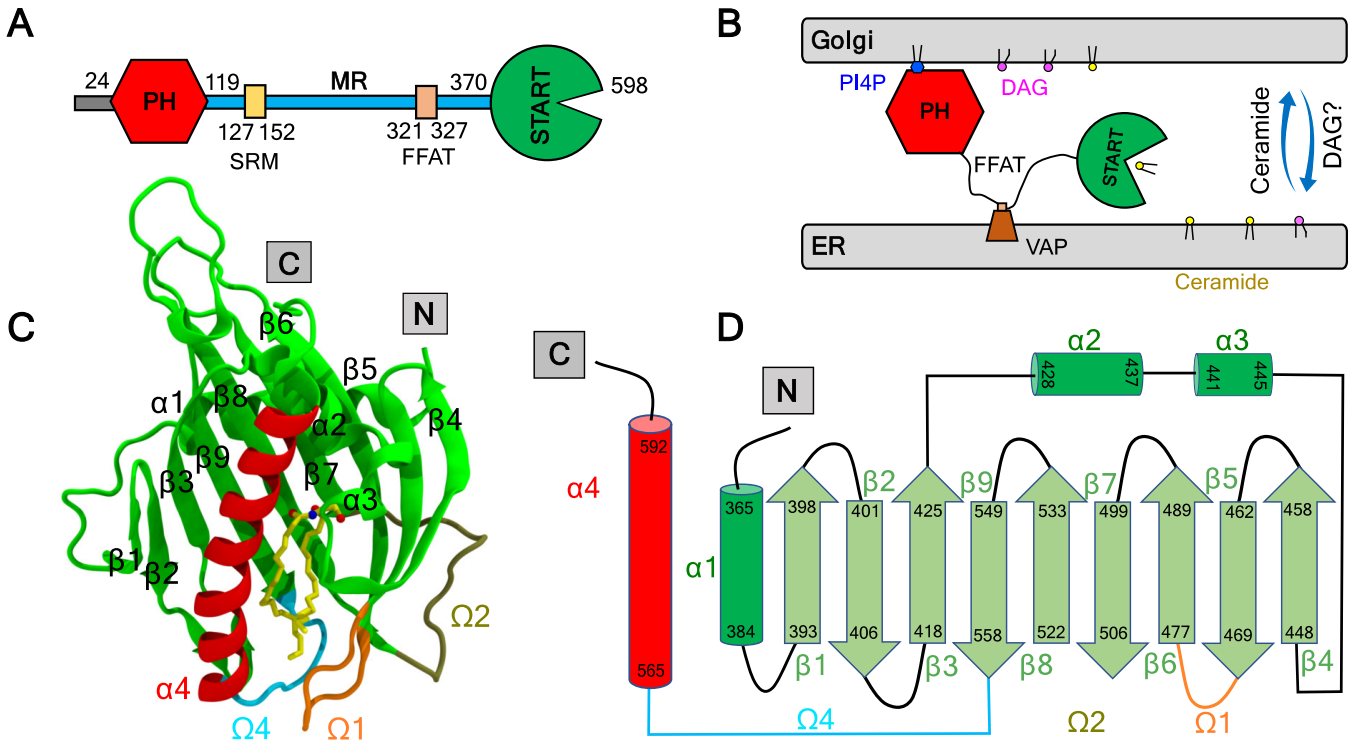

Figure 1. Model of CERT-mediated trafficking of ceramide. (A) Domains and motifs in CERT. The PH domain, START domain, and sequence of the SRM and FFAT motifs are depicted in colored objects, and the MR is shown as a blue bar. (B) Ceramide transfer from the ER to the trans-Golgi membrane. (C) Structure of the START domain in complex with ceramide. (D) Topology diagram of the START domain.

loop is called the Ω1 loop (exchange loop in PITP, Ω in PRELI, and α2 in Ups1). The 27 available X-ray structures of START, in its apo form and bound to ceramide or various other ligands and inhibitors, show a cavity formed by residues of the α4 helix and Ω4 loop on one side (left on Figure 1C) and amino acids from the α3 helix and the Ω1 loop on the other side (Figure 1C, right). The polar head group of Cer is accommodated at the far end of the hydrophobic cavity forming a hydrogen bond network with R442, E446, Q467, Y482, N504, and Y553. The unsaturated sphingosine and saturated fatty acid tails are surrounded by the hydrophobic wall of the cavity, whose size and shape dictate the length limit for cognate ceramides.[15] Kudo et al. suggested that two exposed tryptophan residues, W473 in the Ω1 loop and W562 in the Ω4 loop (β9-α4 loop, Figure 1C,D), might dictate the orientation of START when bound to membranes.[5] They showed that a W473A/W562A double mutant reduces the membrane affinity with reduced ceramide extraction and almost no transfer activities in cell-free assay systems. This mutant of CERT also shows no ER-to-Golgi trafficking of ceramide in semi-intact cells. However, the W473A/W562A CERT mutant retains the ability to localize at the Golgi region, consistent with the idea that CERT can target the Golgi apparatus by recognizing PI4P via its PH domain.[7,16] Structures of START with ceramide-analog inhibitors show a large displacement of the W473 side chain, which moves inside the cavity,[15] while it is exposed to the outside in the apo form and ceramide-bound complexes.

While Kudo et al. suggested that the α3 helix (Figure 1C) and the Ω1 loop of START might function as a gate to the lipid-binding cavity,[5] none of the 27 START structures show an open gate or any notable conformational differences in the region of α3 and Ω1 or in any other regions. As a consequence, the mechanisms controlling the operation of the START gate and the incorporation (or release) of Cer into (or from) the hydrophobic cavity remain poorly understood. Molecular dynamics (MD) simulations, in particular when supported by experimental validation, have the potential to inform about conformational dynamics of membrane-bound proteins at an atomic resolution.[13,17−23] MD simulations have also shed light on membrane binding and conformational changes for other members of the StARkin superfamily.[11,13,24−27] However, the mechanism by which CERT or other StARkin proteins extract/release their lipid cargo across the polar membrane interface into/from the binding site is still unknown. Dennis and co-workers leveraged the potential of molecular dynamics simulations to reveal the critical role of the membrane, akin to an allosteric effector, in facilitating the extraction and binding of phospholipid substrates by the phospholipase A2 enzyme.[17,28,29] It is natural to wonder whether the membrane could also play an important role in lipid cargo uptake and release by lipid transfer proteins and CERT in particular.

To shed light on the CERT membrane binding and ceramide release mechanisms, we used extensive atomistic molecular simulations of the binding of the apo and holo START on complex lipid bilayers mimicking the ER and Golgi membranes, respectively. The simulations performed for each protein−membrane system were extended well beyond the membrane binding events and until two microseconds each to investigate the interplay between the protein, its cargo, and the membrane lipids. The trajectories were thus analyzed with a focus on information pertinent to the opening/closing of the cavity and the behavior of ceramide. We observed a series of diffusive and rare events that favor the release of Cer from the START domain and propose a model where these events

https://doi.org/10.1021/acs.jpcb.4c02398
J. Phys. Chem. B 2024, 128, 6338−6351

combined would lead to full release of Cer from the holo START domain to a Golgi-like lipid bilayer.

MATERIALS AND METHODS

System Preparation for Apo-ER, Holo-Golgi, and Holo-neutral. We retrieved X-ray structures from the Protein Data Bank (PDB)[30] for apo CERT START (PDB ID 2e3m[5]) and holo CERT START (PDB ID 2e3q[5]) domains. The apo and holo structures contain coordinates for amino acids V362−F598 and T364−F598, respectively. The two protein structures were placed above the surface of the relevant lipid bilayers (ER-, Golgi-like, and neutral) built using CHARMM-GUI,[31] explicit TIP3P water molecules,[32] and neutralizing potassium ions. The starting orientation of the protein on the bilayers was obtained from theoretical predictions from the Orientation of Proteins in Membranes (OPM) database.[33] In this orientation, the START domain is positioned with the Ω1 and Ω4 loops facing the bilayer. In addition, we tested three alternative orientations of the protein with either (i) Ω1, β4, and α3, (ii) β1 and β2, or (iii) α1 and Ω2 facing the bilayer (Table S1 and Figure S1). These three orientations were selected based on the three (left-, right-, and back-side) walls surrounding the entrance to the cavity. The orientation with Ω1, β4, and α3 facing the bilayer (left-side wall) was proposed as a gate to the cavity by Kudo et al.[5] Bilayers comprised 256 lipid molecules (128 lipids for each leaflet).

Simulation Protocol. The systems were prepared using CHARMM-GUI.[31,34] All simulations were performed using NAMD (v 2.13)[35] with the CHARMM36 force field[36−38] and its CHARMM-WYF extension for the treatment of aromatics−choline interactions.[39,40] After the protein/membrane complex was assembled, the systems were first subjected to energy minimization with conjugate gradients (10,000 steps). Then, six consecutive equilibrations were performed using the default equilibration protocol of CHARMM-GUI. During 50 ns equilibrations, we had gradual equilibrations of the initially assembled system; various restraints were applied to the protein, ligand, water, ions, and lipid molecules, similar to those used by Jo et al.[41] Next, the production runs were performed for at least 2 μs using the coordinates and velocities of the last step of the equilibration run. All of the production runs were done with an integration step of 2 fs in the NPT ensemble. The temperature and pressure were set at 310 K and 1 bar, respectively. Langevin dynamics with a temperature damping coefficient of 1.0 and the Langevin piston method with an oscillation period of 50 fs and a damping timescale of 25 fs were used to control the temperature and pressure, respectively. The ratio of the unit cell in the $x-y$ plane was kept constant. The SHAKE algorithm was applied to constrain all bonds between hydrogen and heavy atoms, including those in water molecules to keep water molecules rigid.[42] Electrostatic potentials were calculated using the particle mesh Ewald (PME) method.[43] A Lennard-Jones switching function of 10−12 Å was used for van der Waals interactions. For each of the systems, we ran at least two series of simulations independently. The simulation conditions are summarized in Table S1. All simulations were uploaded to the Norwegian National Infrastructure for Research.

Building the Holo-Golgi-POPC System. We used the already formed complex in the holo-neutral simulation (Figure 6A in the Results section) with a POPC tail in the cavity as a reference structure to guide the building of our model complex. First, we extracted a START structure with a ceramide molecule from our holo-Golgi simulation with already broken hydrogen bonds between the bound ceramide and residues at the binding site (Y482, N504, and Y553). We then aligned the model structure to the reference structure and transferred the POPC lipid from the reference holo-neutral simulation. Then, a single-point energy calculation was performed using the CHARMM-GUI PDB Reader & Manipulator.[44] This step ensured that the atomic coordinates were successfully defined and that the structure was ready to use in the CHARMM-GUI Membrane Builder tool.[45] The complex was placed onto the Golgi-like bilayer using the same orientation and penetration depth as those observed in our other simulations. The system was then solvated in a water box and neutralized with 51 K^+ ions. To ensure that the final system had no steric clashes or inappropriate geometry, an energy minimization was performed prior to starting a 2 μs-long dynamics simulation (and a replica) using the same protocol as above.

Simulation Trajectory Analyses. The backbone RMSD between each simulation frame and the solvated and minimized X-ray structure was calculated using VMD[46] and is reported in the Supporting Information (Figure S2). The RMSD was calculated for the bound form of the proteins. The average RMSD for each of the six systems varied from 2.5 to 3.4 Å, a high value mostly accounted for by the mobile N-terminal helix in some simulations. The range of average RMSD values falls to 2.1−2.6 Å if residues 362−392 are omitted from the calculation.

The electrostatic surface potential of START (apo) was calculated using APBS[47] and PyMOL.[48] The protein tilt angle was defined as the angle between the bilayer normal and the long axis of the C-terminus α4 helix, defined by the α carbons of A565 and T591 (Figure S3). The angle and minimum distances were calculated using GROMACS analysis tools[49] for the whole 2 μs simulations. The electron density was calculated using the VMD Membrane Plugin[50] and during the last 500 ns of each simulation. The depth of insertion of the START domain was calculated using in-house Python code for each amino acid as the distance between its β carbon (for glycine α carbon) and the average plane of the phosphorus atoms. The average plane was calculated over the binding to the bilayer to the end of the simulations.

Hydrophobic contacts between atoms are considered to exist if two unbound candidate atoms (Table S2) are within 3 Å for a minimum of two consecutive frames and are present in all replicas. If one or more such contact is detected between atoms of two amino acids (or one aa and a lipid), we consider that these amino acids (or aa and lipid) engage in a hydrophobic contact (e.g., for plot on Figure 5 in the Results section). The candidate atoms for hydrophobic contacts are listed in Table S2. The criteria for hydrogen bonds are the following: an acceptor (A)-to-hydrogen distance of $\leq$2.4 Å and an angle D−H−A (D: hydrogen bond donor) of $\geq$130°. Additionally, these criteria for hydrogen bonds must be met for at least two consecutive frames and present in all replicas. Cation−π interactions between the aromatic amino acids (W, F, and Y) and lipids were considered to exist when all distances between the aromatic ring atoms and the choline nitrogen were below 7 Å. We used an in-house parallel Python3 program to perform the analysis. The code reads DCD trajectory files and can be run on modern multicore computers. The code is based on MDAnalysis[51,52] for parsing of structure and trajectory files and for detection of hydrogen bonds

https://doi.org/10.1021/acs.jpcb.4c02398
J. Phys. Chem. B 2024, 128, 6338−6351

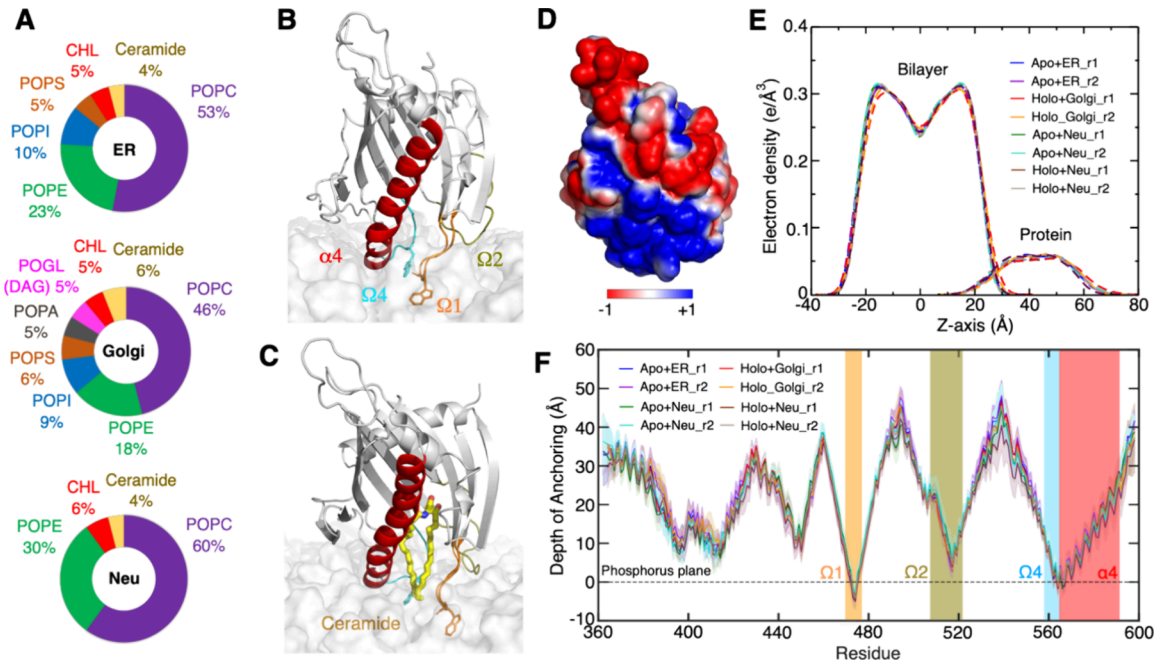

Figure 2. Binding mode of apo and holo START on ER- and Golgi-like bilayers from molecular dynamics simulation. (A) Lipid compositions in ER-, Golgi-like, and neutral bilayers. (B,C) MD snapshots of the bilayer-bound apo and holo START on ER- and Golgi-like bilayers, respectively. (D) Electrostatic surface potential of apo START mapped on the molecular surface (negative: red, positive: blue) (E) Electron density profiles of the bilayers and protein from MD simulations including both replicas (r1 and r2) in each case, calculated for the last 500 ns of the simulations. (F) Depth of insertion of the Cβ of each START amino acid (Cα of glycines) into the bilayers for all systems and replicas, calculated from the time that the START domain binds to the bilayer to the end of the simulations (see Materials and Methods).

(hydrogen bond analysis module). The most computing-intensive part, distance calculation for the detection of hydrophobic contacts, adopts a parallel implementation with Numba [https://numba.pydata.org/] and can be accelerated on multiple CPU cores. The code is available at https://github.com/reuter-group/MD-contacts-analysis. The inventory of protein−lipid hydrophobic contacts, hydrogen bonds, and cation−π interactions was calculated for the bilayer-bound form of START, i.e., from the binding event and until 2 μs.

The gate opening was quantified using the distances between P564 (Ω4) and W473 (Ω1) on the one hand and between W562 (Ω4) and S476 (Ω1) on the other hand. The lipid tail tilt angle with respect to the Z axis was calculated using the vector defined between the C2 and C218/C316. The lipid tail snorkeling was evaluated based on the criterion that the last carbon in the tail is higher than 5 Å below the average plane of the phosphorus atoms ($z > -5$ Å) for more than 1% of the 2 μs simulation.

Free Energy Calculations. Calculations of relative binding free energy were performed using multisite lambda dynamics (MSλD).[53,54] The calculations were performed with the 47a2 version of the CHARMM biomolecular package[55] using either DOMDEC[56] or BLaDE[57] on graphical processing units (GPUs) and the CHARMM36 force field. The protocols used for system preparation and simulation can be found in the Supporting Information (Supplementary Text S1).

Visualization. Visual analysis and image and movie generation were performed using VMD and PyMOL.

Characterization of CERT−Lipid Complexes. CERT (isoform 2) was cloned in frame with a N-terminal His6-HA-Strep IItag in a pcDNA5/FRT/TO vector and checked for expression in HEK293 cells. HEK293 cells were maintained in DMEM, supplemented with 10% (v/v) FBS and 1% L-glutamine, in the presence of 1% Pen/Strep antibiotics mix, for transient expression of the tagged LTP of interest. To create stable inducible human cell lines for LTPs, Flp-In T-Rex-293 cells were cotransfected with the plasmid coding for the tagged LTP and the pOG44 plasmid encoding the Flp recombinase (Invitrogen). Positive clones were selected by adding 100 μg/mL hygromicin B and 15 μg/mL blasticidin on the day after transfection. Before transfection, the cells were kept under selection in the presence of 15μg/mL blasticidin and 100 μg/mL Zeocin. Cells were seeded and grown in the presence of 1 μg/mL tetracycline (without other antibiotics) until 95% confluence, harvested, pelleted, and stored at −80 °C for later use. CERT expression was evaluated by Western blotting with the α-HA antibody, and all cell lines were tested for the presence of mycoplasma.

Cell lysis was performed by resuspending cell pellets in a lysis buffer (50 mM Tris-HCl, 250 mM NaCl, 0.5 mM DTT, 2 μM avidin, 0.5% NP40, protease inhibitor cocktail (Roche), and DNase (Roche), at pH 7.4) and leaving on ice for 20 min. The final cell extract was obtained by centrifugation for 20 min at 16,000g at 4 °C in a benchtop centrifuge followed by centrifugation of the previous supernatant at 49,000 rpm, using a TLA100.4 rotor. Protein−lipid complexes were isolated via the Strep II tag at room temperature and eluted with 5 mM biotin. The eluted complexes were centrifuged at 16,000g for 5 min and fractionated on a Superdex 200 SEC column (Invitrogen). Proteins and lipids in the SEC fractions were analyzed by sodium dodecyl sulfate polyacrylamide gel electrophoresis (SDS-PAGE) on precast 4−12% gradient gel (Life Technologies) and by LC-MS/MS, respectively.

Lipids were separated on an Agilent 1260 HPLC system consisting of a degasser, a binary pump, and an autosampler directly coupled to a Q Exactive Plus (Thermo) equipped with

https://doi.org/10.1021/acs.jpcb.4c02398
J. Phys. Chem. B 2024, 128, 6338−6351

a heated ESI source. The column was a Kinetex 30 × 2.1 mm, 2.6 μm, C18 100 Å (Phenomenex). A binary solvent system was used in order to separate the lipids. The mobile phase A consisted of H_2O:acetonitrile (60:40), 10 mM ammonium formate, and 0.1% formic acid, while the mobile phase B consisted of isopropanol:ACN acetonitrile (90:10), 10 mM ammonium formate, and 0.1% formic acid. The separation started at 80% buffer A and 20% buffer B. In a 3 min gradient, buffer B was increased from 20 to 50% followed by a 10 min gradient from 50 to 70% buffer B. Finally, a 5.4 min gradient was applied to increase buffer B from 70 to 97%. The column was subsequently washed for 2.1 min with 97% buffer B and equilibrated for 3.6 min with 20% buffer B. The flow rate was 500 μL/min. The entire run was 24 min long. The effluent was directly introduced into the ESI source of the MS, and the resulting sample was analyzed each time for each paired fraction in either positive or negative ionization mode. The ESI source ion spray voltage was set to 1.7 kV. The mass spectrometer was operated in the mass range from 250 to 1600 m/z. Charge state screening was not enabled. The 10 most abundant peaks (top 10) were selected and fragmented in MS2 by HCD. The normalized collision energy (NCE) was 30.

RESULTS

Atomistic Molecular Simulations of the START Domain Binding to ER and Golgi Membrane Models. We performed molecular dynamics simulations of the apo and holo forms of START in the presence of all-atom bilayers mimicking the composition of the ER and Golgi membranes.[58] These bilayers are hereafter named ER and Golgi bilayers, and their lipid compositions are depicted in Figure 2A. The main difference between the two is the presence in the Golgi-like bilayer of cone-shaped lipids,[59,60] diacylglycerol (DAG) and phosphatidic acid (PA), which can decrease the packing of the polar head groups.[61] Meanwhile, phosphatidylcholine (PC), phosphatidylethanolamine (PE), phosphatidylinositol (PI), phosphatidylserine (PS), and cholesterol (CHL) are present in both; 1-palmitoyl-2-oleoyl (PO) chains were used for all lipids. The chosen lipid compositions represent a simplification of *in vivo* membranes. We also used a simpler neutral bilayer consisting only of PC, PE, CHL, and Cer. In what follows, the simulation of the apo form on the ER-like bilayer is named apo-ER, and the simulation of the holo form on the Golgi-like bilayer is named holo-Golgi.

The protein structure was initially positioned slightly above the bilayers and oriented with the Ω1 and Ω4 loops facing the bilayer. Control simulations were performed with three alternative orientations, as described in the Supporting Information (Figure S1). Each simulation was run for a total of 2 μs and replicated once (Table S1). Apo and holo START domains were bound spontaneously within 300 to 500 ns onto the ER bilayer and within 60 or 500 ns on the Golgi bilayer depending on the replicate. All simulations led to the same bound orientations, as shown in Figure 2B,C and Figure S1. The structures remained close to the X-ray structures except for the N-terminal region, which was highly mobile. In the full CERT protein, this region links to the FFAT motif and further to the MR domain, and the absence of this domain in the simulations might explain the high mobility observed. In addition, we observed changes in root-mean-square deviation (RMSD) (Figure S2) following the binding of START to the bilayers and corresponding to gate opening events that are described in detail in the next sections.

The Ω1 and Ω4 Loops Anchor the START Domain to ER- and Golgi-like Bilayers. To characterize the orientation and the depth of insertion of START on the bilayers, we calculated the electron density of protein and lipids along the direction perpendicular (normal) to the membrane plane (Figure 2E), the angle between helix α4 and the membrane normal (Figure S3), the minimum distance between the START domain and the bilayers (Figure S4), the distance between the β carbon of each amino acid (except for glycine in which α carbon is used), and the average plane of the phosphorus atoms in the upper leaflet (Figure 2F).

The insertion depth and orientation of apo START on the ER bilayer are similar to those of holo START on the Golgi bilayer. There are no notable changes in the tilt angle upon binding of START to the bilayers, and the angle remains around its average value of 40 ± 15° for the ER and Golgi bilayers (Figure S3). For both types of membranes, START (apo on ER and holo on Golgi) is anchored rather superficially to the bilayers (Figure 2E) through the C-terminus α4 helix and the Ω1, Ω2, and Ω4 loops (Figure 2F). Only a few residues are inserted under the average plane of the phosphorus atoms (Figure 2F). This is also reflected in the inventory of interactions between START amino acids and bilayer lipids (Table S3). Helix α4, Ω1, and Ω4 mediate hydrophobic contacts with multiple lipid tails mostly through the same amino acids in both bilayers: W473 (Ω1) and W562 (Ω4) and a few hydrophobic amino acids V472 and P474 in Ω1, V562 and P564 in Ω4, and V571 in α4. Helix α4 and Ω1 and Ω4 loops also engage in several long-lasting hydrogen bonds with the lipid head groups, mostly with the phosphate groups. Six basic amino acids are involved: R471 in Ω1, R478 in β6 (right after Ω1), R569, K573, R574, and K578 in α4. In addition, we observe hydrogen bonds with R517 in the Ω2 loop. Unlike what we have observed for other proteins,[62] there are no long-lasting cation−π interactions between aromatic amino acids and choline head groups.[63] The two exposed tryptophan residues, W473 and W562, engage in hydrophobic contacts with the fatty acid tails and hydrogen bonds with the phosphate and glycerol groups of the membrane lipids. W473 is inserted deep in the bilayer forming hydrogen bonds with the lipid glycerol group, while W562 mostly forms hydrogen bonds with the lipid phosphate groups (Table S4).

The electrostatic surface potential of the START domain (Figure 2D) shows a positive region at the membrane binding site suggesting an electrostatic recognition of the ER and Golgi bilayers, which both contain negatively charged lipids. We evaluated the influence of the surface charge of the bilayers on protein binding by performing a control simulation with an ER bilayer stripped from its negatively charged lipids (Neu, Figure 2A). There was no difference in the depth of insertion (Figure 2E,F) or the orientation (Figure S3) of START on the neutral Neu bilayer compared to that of the ER and Golgi bilayers, ruling out a dominating electrostatic contribution in START membrane binding. Overall, our data suggest that the START domain has general affinities with membranes and that this domain alone is not sufficient to target specific lipids or bilayers. This function is probably mediated by the PH domain, the SRM, and/or FFAT motifs of CERT.

The Opening of Ω1 and Ω4 Loops Triggers Snorkeling of Lipid Tails under the Hydrophobic Cavity of the START Domain. Visual inspections of simulations of START (apo and holo) on the ER and Golgi bilayers revealed an opening of the gate to the ceramide binding pocket through

https://doi.org/10.1021/acs.jpcb.4c02398
J. Phys. Chem. B 2024, 128, 6338−6351

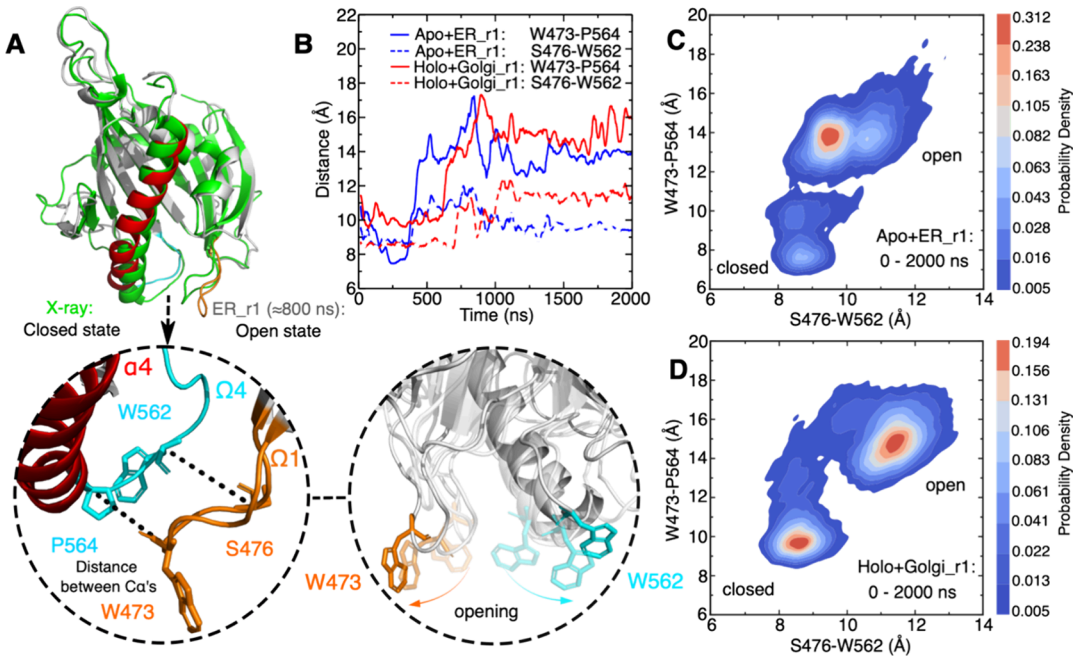

Figure 3. Gate opening through displacements of Ω1, Ω4, and α4. (A) Superimposition of the open state in gray cartoon (α4 in red, Ω1 in orange, Ω4 in cyan, and MD snapshot at ≈800 ns of apo+ER_r1 simulation) with the closed state in green cartoon (X-ray structure, PDB ID 2e3m) and close-ups of the open state and of the orientation of the tryptophan W473 and W562 side chains along a simulation. Hydrogens are not shown for the sake of clarity. (B) Time series of the W473−P564 (plain lines) and S476−W562 (dotted lines) distances in simulations of START with the ER (blue) and Golgi (red) bilayers (see Figure S5 for the replicas). (C,D) Estimated probability density (KDE function) of the closed and open states of START calculated from the simulation trajectories with the ER bilayer (C) or Golgi bilayer (D). KDE (kernel density estimation) represents the data using a continuous probability density curve. The bar at the right side shows the intensity of data values along the KDE curve.

displacements of the N-terminal end of helix α4 and of loops Ω1 and Ω4. The change was not observed in the second replica of the START-ER simulation. The conformational change is illustrated in Figure 3A with a snapshot taken at $t \approx$ 800 ns of the simulation of the apo form of START on the ER bilayer. Shortly after the binding of START onto the bilayers, α4 and the Ω1 and Ω4 loops undergo a large structural shift, leading, among other things, to the disruption of interactions between the two loops (Figure S6). The gate opening is quantified in Figure 3B by time series of the distances between P564 (Ω4) and W473 (Ω1) on the one hand and W562 (Ω4) and S476 (Ω1) on the other hand (see Figure S5). Furthermore, Figure 3C,D shows the distributions of the closed and open states of the START domain on the ER and Golgi bilayers. The average distances of the P564 (Ω4) and W473 (Ω1) residues to the Golgi bilayer are 9.5 and 15 Å for the closed and open states, respectively. Upon opening of the gate, the side chains of W473 and W562 shift toward the outside of the cavity, resulting in a fully open state (Figure 3A).

We also performed a 1 μs-long simulation of the START apo form in water and replicated it twice. The analysis of these simulations, specifically the time series of the START domain opening distances (Figures S7 and S8), demonstrates the occurrence of opening events similar to those observed in the membrane-bound START domain. However, these events have a short duration of only 100 ps. This indicates a role of the membrane lipids in stabilizing an opened form of the gate, rather than triggering it.

START opening exposes the hydrophobic lipid-binding pocket to the hydrophobic environment of the bilayer. In the simulation of the apo START on the ER bilayer and of the holo form on the Golgi and neutral bilayers, the opening of the gate is concomitant to a change of the neighboring lipid tails that tend to snorkel in the space just under the opened hydrophobic cavity (Figure S9). This is illustrated by the simulation snapshots in Figure S9 and quantified by monitoring the distance between the last carbon atoms of the lipid tails and the average position of the phosphate groups, projected onto the normal to the bilayer (with respect to the Z axis) (Figure S10). From the gate opening event in the apo +ER_r1 simulation and for as long as it is opened, we observe between 3 and 4 lipids positioned under the gate and whose tail deviates from the orientation of other lipids. For the sake of comparison, the average number of lipids undergoing such conformational changes in the whole opposite leaflet (i.e., in the absence of protein) is between 1 and 2 (Figure S11). Interestingly, in the holo-Golgi simulation, these events led to the bound ceramide to extend its tails toward the bilayer, increasing the number of contacts between ceramide and lipid tails from 0 to 10−16 before and after gate opening in the first simulation and from 0 to 20−24 contacts in the replicate (Figure S12).

POPC Tail Insertion Triggers Release of Ceramide. In addition to the frequent local molecular rearrangements of proteins and the lipid tails in the bilayers described above, we observed the engagement of a POPC (palmitoyl-oleoyl-PC) lipid in the hydrophobic cavity. That POPC lipid inserts one tail into the hydrophobic cavity in one replicate of each of the apo-ER, apo-neutral, holo-neutral, and holo-Golgi simulations (see Supplementary Text S2 for other replicates). This phenomenon is illustrated by the snapshots in Figure 4 and Figure S13. The orientation of the inserted tail is quantified by its angle with the membrane normal (Figure 4B,D and Figure 13B,D). In each of the four simulations, a POPC phosphate

https://doi.org/10.1021/acs.jpcb.4c02398
J. Phys. Chem. B 2024, 128, 6338−6351

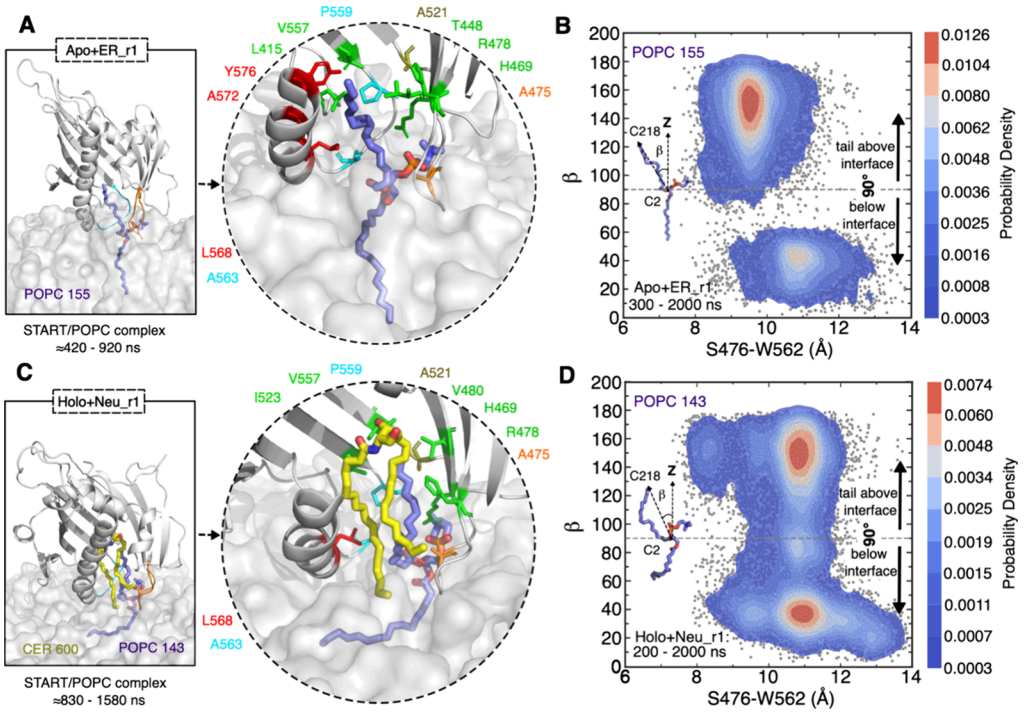

Figure 4. POPC (1-palmitoyl-2-oleoyl-phosphatidylcholine) rearrangement induced by the START domain in the open state detected by MD simulation. (A) Close-up view of the binding conformation of POPC within the apo START domain and the amino acids in the cavity involved in hydrophobic contacts with the POPC tail in the ER bilayer. The START domain is shown as gray cartoons with Ω1 in orange and Ω4 in cyan, ceramide and POPC as yellow and purple sticks, respectively, and the bilayer as a gray transparent surface. The times at which the POPC tail inserts into and exits the cavity are given below the snapshots. (B) Distribution of the POPC tail angle with respect to the membrane normal in the ER bilayer and their estimated probability density (KDE function) are presented. The gray dots represent all the sampled tilt angles. (C) Close-up view of the binding conformation of POPC within the START-Cer complex and the amino acids in the cavity involved in hydrophobic contacts with the POPC tail in the neutral bilayer. (D) Distribution of the POPC tail angle with respect to the membrane normal in the neutral bilayer and their estimated probability density (KDE function) are presented. The KDE represents the data by using a continuous probability density curve. The bar at the right side shows the intensity of data values along the KDE curve.

group is locked in the gap between the opened Ω1 and Ω4 loops by a salt bridge with R478 and hydrogen bonds with the S476 (Figure S14). One tail of that POPC engages in hydrophobic contacts with exposed amino acids at the entrance of the cavity and shifts toward the hydrophobic core of the cavity to finally insert into it (Figure 4A,C and Figure 13A,C). The tail angle then changes from high values when the tail is in the bilayer (above 150°) to low values characteristic of the insertion in the cavity (45° and below). There are slight differences in the four simulations. In three of the simulations (apo-ER, apo-Neu, and holo-Neu), the unsaturated tail is inserted, while the saturated fatty acyl chain stays in the membrane. In the fourth simulation (holo-Golgi), it is the saturated tail that moves toward the gate, but it adopts a somewhat different position from the unsaturated tail in the other three simulations. Indeed, it interacts mostly with the Ω1 loop at the entrance of the cavity (Figure S13C), unlike in the other three cases where it interacts with residues located deep in the cavity (Figure 4A,C and Figure S13A). The lifetime of the START-POPC complex is short in the holo-Golgi (40 ns) and apo-Neu (70 ns) simulations but longer in the apo-ER (500 ns) and holo-Neu (750 ns) simulations (see Movies S1, S2A, S2B, and S3).

Following the insertion of a POPC tail into the cavity in one of our simulations of the START-Cer complex (holo-Neu, Figure 4C), we observed a temporary release of ceramide from the cavity and into the lipid bilayer (Figure 5A−F). The POPC tail intercalates between the protein and the ceramide. The time series of the hydrophobic contacts before and after the tail insertion shows a disruption of the protein−ceramide hydrophobic contacts (with R478, V480, A521, I523, V557, and P559) and the formation of contacts between these residues and the POPC (Figure 5H,I). The hydrogen bonds between the ceramide head group and its binding site (Y482, N504, and Y553) then break sequentially (Figure 5G). This step is followed by the release of ceramide, which inserts between other lipids in the bilayer (Figure 5E and Figure S12). It is followed by the exit of the POPC lipid tail from the cavity ($t \approx$ 1580 ns). Subsequently, the ceramide moves back up to the cavity (Figure 5F), but its head group fails to re-establish a stable hydrogen bond network with Y482, N504, and Y553. Instead, the ceramide slides back and forth along the long axis of the cavity for the remaining simulation time (Movie S2C).

We observe other lipids between Ω1 and Ω4 during our simulations, such as POPE (palmitoyl-oleoyl-PE) or POPS (palmitoyl-oleoyl-PS) but no other lipid than PC inserts a tail in the cavity. Like POPC, the PE and PS lipids form hydrogen bonds with neighboring amino acids (S476, R478, and W562), but unlike POPC, their head groups (ethanolamine and serine) are engaged in long-lasting interactions. These interactions are likely to explain the limited degrees of freedom of the bound PE and PS lipids that we observe and the apparent restricted mobility, which hinders the insertion of their tails in the hydrophobic cavity.

Our observations from the holo-neutral and holo-Golgi bilayers suggest that the ceramide release is triggered by a

https://doi.org/10.1021/acs.jpcb.4c02398
J. Phys. Chem. B 2024, 128, 6338−6351

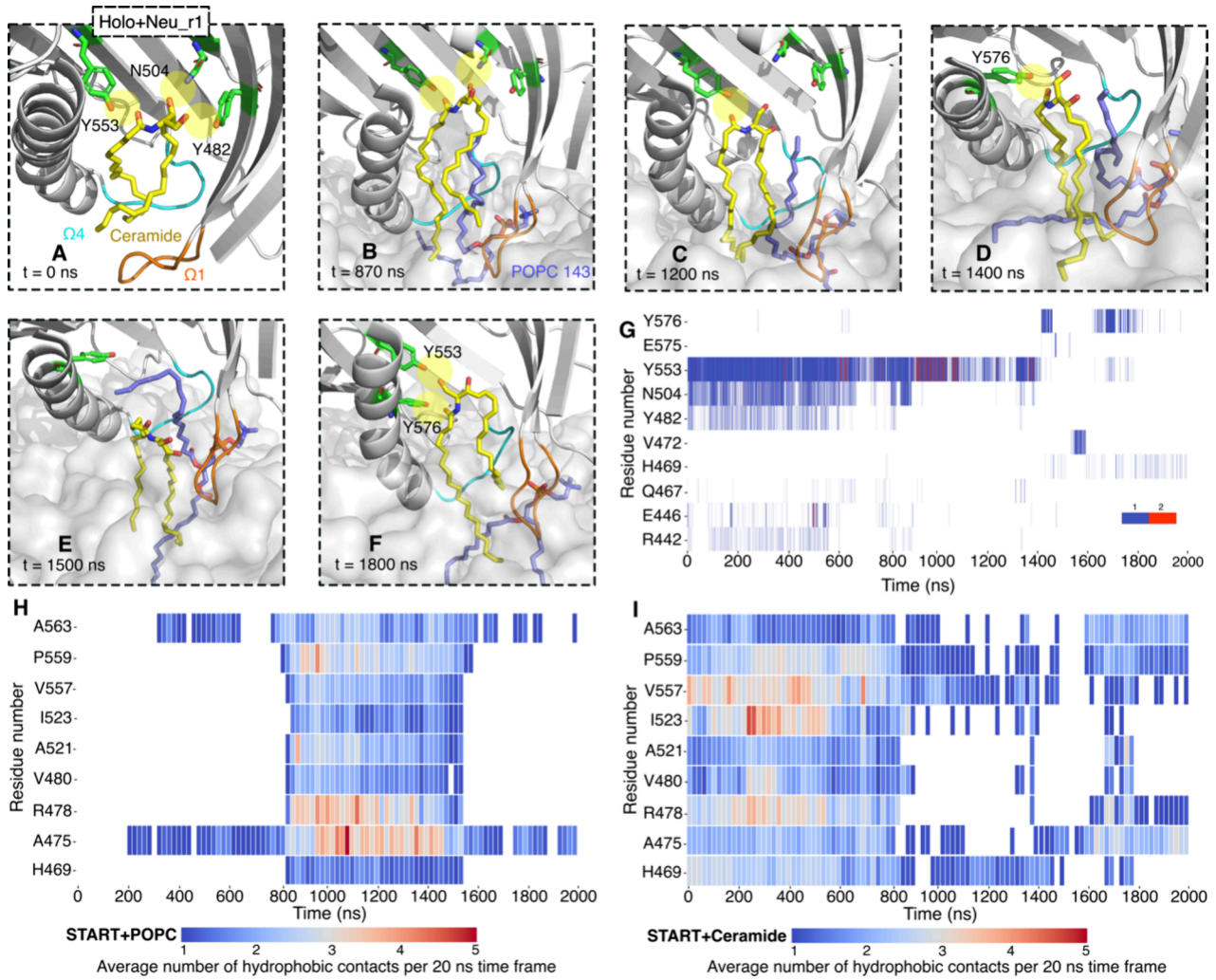

Figure 5. Snapshots along 2 μs simulations of holo START on the neutral bilayer. (A) Hydrogen bond network between the ceramide and cavity residues (green licorice, yellow highlight for hydrogen bonds) before binding to the bilayer. (B,D) Hydrogen bonds break one by one, and the Cer is displaced from the binding site, forming a hydrogen bond with Y576 of the C-terminus α4 as the Cer moves toward the bilayer (see Figure S15 and Table S5 for other replicates). (E) The POPC143 tail disrupts the Cer-Y576 hydrogen bond. (F) Cer forms hydrogen bonds again with Y553 and Y576 as the POPC tail leaves the cavity. (G) Time series for the hydrogen bond network between ceramide and the START domain. The color bar indicates the number of hydrogen bonds in each frame. (H,I) Time series of the average number of hydrophobic contacts for selected residues, calculated in 20 ns time windows, throughout the 2 μ simulations: (H) POPC143 with the protein and (I) ceramide with the protein (see Figure S16 for all the hydrophobic contacts). Ceramide, colored yellow; POPC, colored purple; Ω1, colored orange; Ω4, colored cyan. The START domain is shown as a cartoon and colored gray. The membrane is shown as a gray transparent surface.

succession of events: (1) the hydrophobic cavity is stabilized in its open form by the lipid bilayer, (2) the ceramide exposed tails are in contact with bilayer lipids, (3) bilayer lipid tails snorkel around the open cavity, and (4) a POPC tail is inserted deep into the cavity (such as in the holo-neutral simulation). Steps (1)−(3) occur in every simulation replicate, while step (4) is observed in half of the replicates, suggesting that it might be a diffusive rare event (other replicates are reported in Supplementary Text S2).

Verifying that POPC Intercalation between Ceramide and START Disrupts Protein−Ceramide Interactions and Triggers Cargo Release. We first evaluate the effect of the loss of START-Cer interactions on the stability of the complex. The head group of ceramide forms hydrogen bonds with the START domain (Figure 5B,G), and the ceramide tail forms hydrophobic contacts with several amino acids (Figure 5I). The simulation results show a gradual disappearance of these interactions, partly under the influence of the inserted POPC tail but also prior to it. We here evaluate the contribution of a selection of these interactions to the START-Cer affinity to verify that their disappearance is likely to modify the stability of Cer in the START cavity and favor its release. First, we calculated the contributions to the START-Cer binding affinity of the Y553 and N504 hydrogen bonds and of the V480 hydrophobic contact to Cer. This was done by calculating the energy change associated with the Y553F, N504A, and V480A substitutions, in the presence and absence of ceramide (see the Methods section and Tables S6 and S7). We find that the cost of the Y553F and N504A substitutions is 0.8 and 1.1 kcal/mol, respectively, as expected from losing a hydrogen bond.[64,65] This confirms the favorable contribution of Y553 and N504 to START-Cer affinity. The V480A substitution yields a positive free energy difference (1.2 kcal/mol), indicating a loss of affinity caused by the removal of the valine side chain, consequently suggesting a contribution of 1.2 kcal/mol to the START-Cer affinity. When the POPC tail is

https://doi.org/10.1021/acs.jpcb.4c02398
J. Phys. Chem. B 2024, 128, 6338−6351

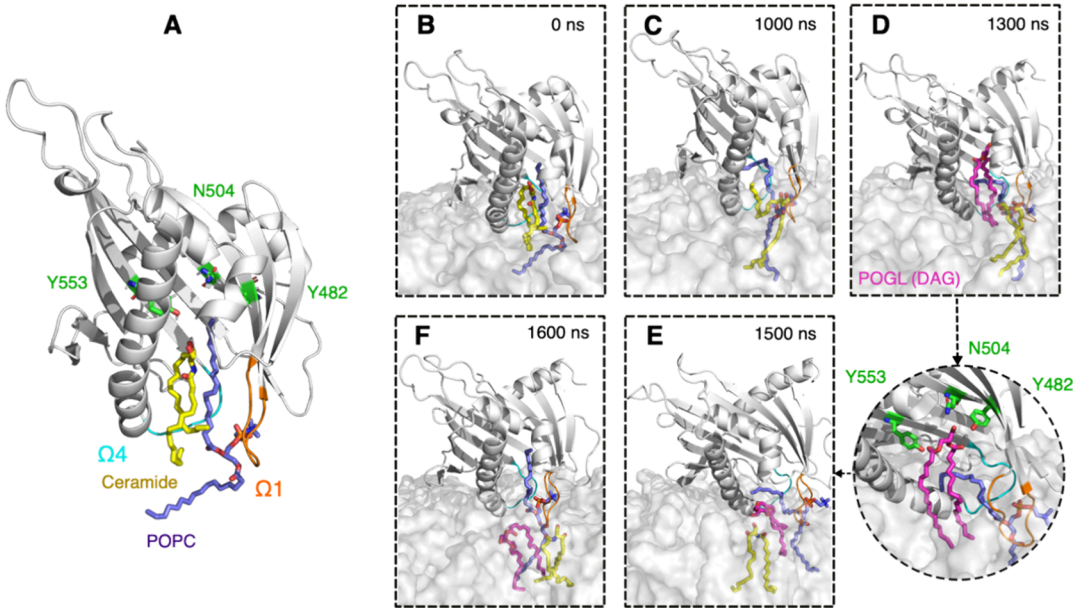

Figure 6. Stages of membrane binding and ceramide release in the model system (Golgi bilayer). (A) Built initial complex of START, ceramide, and POPC. (B,C) Ceramide release to the bilayer. (D−F) Diacylglycerol lipid (POGL) uptake (and release) from (to) the bilayer. Bound ceramide molecule, colored yellow; POPC molecule, colored purple; residues in the binding site, colored in green. POGL is shown in magenta and bound in the cavity. Ω1 loop, colored orange; Ω4 loop, colored cyan; START domain, colored gray. The membrane is shown as a gray transparent surface.

present in the cavity, the V480A substitution yields a negligible affinity loss (0.1 kcal/mol), indicating that V480 does not contribute to the protein−Cer affinity anymore. Overall, these data indicate that the three amino acids contribute favorably by about 1 kcal/mol to the START-Cer binding affinity, and so, their loss is likely to weaken the affinity of Cer for START. We show that the insertion of the POPC tail in the cavity disrupts one of the hydrophobic START-Cer contacts (V480); the associated loss of the contribution to the START-Cer affinity is expected to be of the same order of magnitude for other hydrophobic contacts disrupted by the POPC tail insertion.

As another verification of our proposed model of POPC interfering with the START-Cer interactions, we built a slightly modified holo-Golgi system. We positioned the POPC tail similarly to that which led to the temporary Cer release in the holo-neutral simulation and is shown in Figure 5A−E (seeMaterials and Methodsfor information about model building). We then subjected the model to a 2 μs MD simulation in the presence of the Golgi-like bilayer and replicated the calculation once. In both replicates, the ceramide fully leaves the cavity and enters the bilayer where it mixes with other lipids. Figure 6 shows the initial structure (open form, Figure 6A) anchored to the bilayer (Figure 6B). Within 100 ns, the hydrocarbon tails of the ceramide engage in interaction with the lipid bilayers, and within 1 μs of the simulation (500 ns in the second replicate), the ceramide is fully released into the bilayer (Figure 6C). Notably, we also observe the uptake of a POGL lipid in one of the replicates (Figure 6D−F), but it is released within 200 ns into the bilayer (Movie S4). These simulations confirm that when inserted in a position that weakens the Cer-START interactions quantified above, the POPC lipid will trigger the release of the ceramide cargo on the Golgi-like bilayer.

Biochemical Characterization of PC Binding to CERT from HEK293 Cell Extracts. The in silico models suggest that CERT-mediated ceramide transport requires direct interaction with phosphatidylcholine in the membrane and temporarily at least partial uptake in its hydrophobic cavity. As binding to PC is new, we set out to validate this experimentally by integrating and reanalyzing data from our recent systematic biochemical analysis of LTP cargos.[66] We overexpressed CERT in HEK293 cells and, after biochemical purification, characterized CERT-associated lipids by LC-MS/MS-based lipidomics (Figure 7). We have identified PC (34:1) and PC (32:1) to form stable complexes with CERT (Table S8). Importantly, the MS intensities were similar to those seen with known PC binders, supporting the notion that those interactions do not represent a nonspecific general background. Indeed, PC being the most abundant lipid in eukaryotic membranes, excluding artifacts, was important.

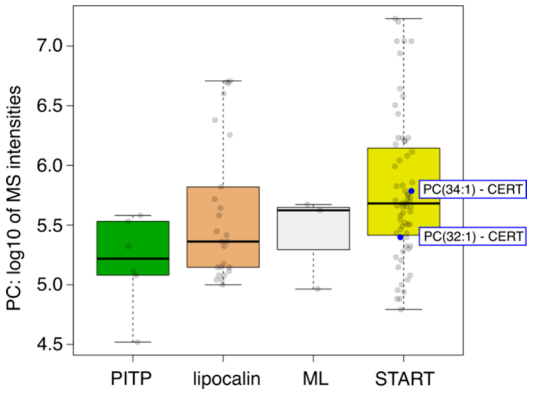

Figure 7. CERT expressed in HEK293 cells forms complexes with PC. Biochemical purification and characterization of CERT−lipid complexes are carried out by LC-MS/MS-based lipidomics. Comparison of the PC binding capacities of CERT with that of other LTPs known to form complexes with PC and belonging to the PITP family (PITPNA and PITPNB), lipocalin family (LCN1), ML family (GM2A), and START family (STARD2, STARD10, and CERT).

https://doi.org/10.1021/acs.jpcb.4c02398
J. Phys. Chem. B 2024, 128, 6338−6351

These experiments provide no information on the stoichiometry of the complex and support the idea that CERTs bind ceramide and PC simultaneously and/or individually. This is the first observation of the association of PC with CERT from a cellular context.

DISCUSSION

Herein, we report a series of extensive unbiased MD simulations of the CERT START domain on lipid bilayers whose lipid compositions mimic those of the cytoplasmic leaflets of the Golgi apparatus and the endoplasmic reticulum. Lipid transfer mechanisms rely on the concomitant occurrence of multiple diffusive and rare events, and the likelihood of observing all required events concurrently within the time frame of unbiased μs-long MD simulations is low. Combining detailed analysis of the MD trajectories with free energy calculations and experimental data, we are able to propose a mechanistic model for the interfacial processes leading to ceramide release by the CERT START domain at the Golgi membrane. In this model, the membrane plays a major role in both the gate opening and cargo release.

According to our simulations, the membrane binding site of the START domain consists of the Ω1 loop, the N-terminal end of helix α4, and the Ω4 loop. Hydrophobic amino acids in these three regions engage in hydrophobic contacts and hydrogen bonds with the lipids. This is in agreement with experimental data[5,15] and in particular the reduction of membrane affinity observed for the START W473A mutant and for the double mutant W473A/W562A and the drastic effect that it has on ceramide transfer.[5] W473 (Ω1) and W562 (Ω4) are observed to engage in long-lasting interactions with lipids in our simulations. Interestingly, we do not observe differences in the membrane binding orientation of the apo and holo forms of the START domain, and the orientation is not sensitive to the lipid composition of the bilayer, indicating a lack of lipid specificity by the START domain itself. This is compatible with the fact that CERT, in addition to its START domain, contains the PH domain and FFAT motif, which ensure targeting of the correct membranes.[4,67]

Our results suggest that Ω1 and Ω4 form the gate through which the cargo enters and leaves the hydrophobic cavity. We observe spontaneous opening of the Ω1 and Ω4 loops, accompanied by movements of the N-terminal end of helix α4, following membrane binding. Upon opening, W473 and W562 undergo a large structural shift toward the outside of the cavity, thus exposing the hydrophobic pocket and the bound ceramide to lipids from the bilayer. In the absence of lipid bilayers, i.e., when the START domain is simulated in water, we observe only transient short-lived opening events indicating a major role of the membrane in maintaining the open state. This would explain the difficulty in observing the open state with structure resolution methods, where no membrane is present. The membrane-bound orientation and opening that we observe are comparable to those reported for PRELID-TRIAP1[13] but do not match with the hypothesis that the Ω1 loop and the α3 helix might function as a gate to the cavity.[5] We do not observe an involvement of α3 in contacts with the bilayer lipids or any notable structural changes that would indicate an involvement of α3 in modulating the access to the cavity. Yet, our observation of the engagement of W473 (Ω1) and W562 (Ω4) in membrane binding and gate opening aligns with the importance of these two residues in the ceramide transfer mechanism.[5,15]

Following the opening of the gate, the lipids located below the START domain undergo a reorientation of their tails, which will snorkel toward the hydrophobic cavity. On the Golgi-like, ER-like, or Neu bilayers, we observe a POPC lipid tail inserting into the hydrophobic cavity, while the polar head group interacts with S476 and R478 maintaining the lipid between the Ω1 and Ω4 loops. Interestingly, S476 (Ω1) is conserved in STARD2-6, and R478 (β6) is conserved in all START domains, except STARD13 (H) and STARD14 (Q). Lipid snorkeling is a known phenomenon that has been observed in both homogeneous POPC and very complex brain membranes. It is thought to be favored in heterogeneous membranes and is correlated with increasing degrees of unsaturation in the hydrocarbon chains as well as a longer tail length.[68] MD simulations of the ceramide-1 phosphate transfer protein have also shown that the protein can induce lipid tail snorkeling, which in turn promotes insertion of lipid tails in the LTP binding sites for a cargo that is thought to be loaded with its hydrocarbon chains first.[69,70] In our simulations, the POPC tail insertion is a catalyst for the cargo release by weakening the interactions between START and its cargo Cer and a displacement of the cargo down toward the lipid bilayer. In two simulations, we observe a spontaneous release that can be summarized as two consecutive events: (1) the inserted tail disrupting the hydrophobic packing between the bound ceramide and the cavity and weakening the Cer-START affinity and (2) a disruption of the hydrogen bond network between ceramide and the three amino acids S482, N504, and Y553.

Interestingly, we could not observe a full ceramide release in the presence of an inserted POPC tail in the simple POPC:POPE:CHL:Cer membrane, while it happened on the Golgi-like bilayer. The timescales of our simulations and the rarity of the release event do not allow us to firmly conclude on a preference for release at the Golgi membrane compared to the ER membrane. As a reminder, the Golgi-like bilayer contains a diacylglycerol (POGL) and the negatively charged lipids POPI, POPS, and POPA and more ceramide than the ER-like and neutral bilayers. One would expect that the presence of conical lipids (POPA and POGL) and a higher concentration of ceramide increases the accessibility to the lipid tails,[71−74] which in turn might facilitate insertion of the cargo in the membrane by increasing its interfacial hydrophobicity as reported by Rogers et al.[75]

The transfer activity of LTPs is thought to be influenced by the lipid composition of the donor and acceptor membranes.[76−79] Moreover, it has been suggested that CERT extracts ceramide from a ceramide-enriched platform.[80] The membrane environment affects the lipid miscibility and interaction with neighboring lipids, as well as the ability of the proteins to scan the membrane surface for the target lipid.[80] Our observations indicate that the protein itself strongly influences the local lipid packing upon binding to the bilayers. It induces changes in the organization of lipids, which form a hydrophobic pool under the protein, surrounded by lipid head groups. This interfacial hydrophobic pool provides a nonpolar environment that shields the hydrophobic lipid tails from contact with water or the polar head groups of the membrane lipids. This results in looser lipid packing, increased mobility of the lipid tails toward the open hydrophobic cavity, and snorkeling, as well as increased interfacial hydrophobicity as also shown in other studies.[69,70,75]

https://doi.org/10.1021/acs.jpcb.4c02398
J. Phys. Chem. B 2024, 128, 6338−6351

Interestingly, the binding and opening mechanisms of the START domain do not appear to be influenced by lipid composition, suggesting the domain's lipid-insensitive nature. However, the cargo release mechanism indicates sensitivity to the membrane lipid composition, implying a potential role of the membrane in the release of the ceramide. It is logical to assume that other domains within the CERT may be responsible for regulating membrane binding and potentially modulating the orientation of the START domain relative to the membrane. Notably, the MR domain contains distinct regions and motifs, such as the FFAT motif and phosphorylation sites, which play crucial roles in CERT function and regulation.[81] Additionally, the interaction of the PH domain with PI4P in the Golgi membrane is essential for maintaining CERT at the Golgi surface wherein CERT releases its ceramide at a certain threshold of the ceramide level.[80] The dependence on PC in the Golgi membrane for the release of ceramide as a cargo from CERT also necessitates their presence at the same location at the same time. This is particularly interesting because PC and ceramide are known substrates for sphingomyelin synthase, which is already known to be downstream of the ceramide transport by CERT. This could furthermore be consistent with the hypothesis that CERT could act as a chaperone, a notion already proposed for the CRAL-TRIO family of LTPs,[82] potentially bringing both substrates to the same location and coupling the transfer to their transformation into sphingomyelin. Together, it seems that the CERT binding and lipid transfer mechanisms are regulated by many factors that we are only beginning to understand.

Following the full release of ceramide into our Golgi-like bilayer, we observed the extraction of POGL from the bilayer. POGL structurally resembles ceramide and is produced as a byproduct in the synthesis of sphingomyelin wherein the phosphorylcholine head is transferred from phosphatidylcholine to ceramide, liberating POGL. It has been shown that the CERT START can transfer diacylglycerol in vitro but with a lower efficiency (only 5%) of the ceramide, suggesting that CERT might mediate Golgi-to-ER trafficking of DAG in exchange for ER-to-Golgi trafficking of ceramide.[48,49] Our simulations show that POGL can be accommodated within the CERT START cavity, although it does not remain in the cavity for long. This return to the bilayer could be due to the presence of the POPC tail in the cavity, which itself facilitates the POGL release process.

CONCLUSIONS

Little is known about the atomistic-level mechanisms by which LTPs extract and release lipids from cellular membranes, or even from simpler in vitro vesicle models, because these events do not lend themselves well to experimental investigations. Molecular dynamics simulations have the potential to provide mechanistic models and generate hypotheses testable experimentally.[13,17−23] Microsecond-long molecular dynamics simulations of START in the presence of lipid bilayers led us to propose a membrane-assisted model of ceramide release from CERT where (i) the membrane lipids stabilize the gate in an open form exposing the large hydrophobic cavity to the membrane interface leading to (ii) an increase of local lipid disorder and (iii) the intercalation of a single PC lipid in the cavity facilitating the passage of the cargo hydrophobic chains through the polar membrane interface, practically greasing its way out. We then set out to experimentally challenge the last step and verified that phosphatidylcholine lipids can indeed form stable complexes with CERT. Altogether, our results underline the critical active role played by the membrane lipids in CERT binding and cargo release. Further investigations will be needed to evaluate a potential generalization of the proposed mechanism to other members of the StART family, which, given their fold similarity, may be operating in a similar fashion.

ASSOCIATED CONTENT

Data Availability Statement

All the MD trajectories are uploaded to the Norwegian National Infrastructure for Research Data (NIRD), have been issued a DOI (10.11582/2023.00139), and can be accessed using the following URL: 10.11582/2023.00139.

Supporting Information

The Supporting Information is available free of charge at https://pubs.acs.org/doi/10.1021/acs.jpcb.4c02398.

Supplementary text, tables, and figures for experimental analysis, MD simulations, and free energy calculations (PDF)

Movies of MD simulation trajectories (ZIP)

AUTHOR INFORMATION

Corresponding Author

Nathalie Reuter − *Department of Chemistry and Computational Biology Unit, Department of Informatics, University of Bergen, Bergen 5020, Norway;* orcid.org/0000-0002-3649-7675; Email: nathalie.reuter@uib.no

Authors

Mahmoud Moqadam − *Department of Chemistry and Computational Biology Unit, Department of Informatics, University of Bergen, Bergen 5020, Norway;* orcid.org/0000-0002-3456-5064

Parveen Gartan − *Department of Chemistry and Computational Biology Unit, Department of Informatics, University of Bergen, Bergen 5020, Norway*

Reza Talandashti − *Department of Chemistry and Computational Biology Unit, Department of Informatics, University of Bergen, Bergen 5020, Norway*

Antonella Chiapparino − *European Molecular Biology Laboratory, EMBL, Heidelberg D-69117, Germany*

Kevin Titeca − *European Molecular Biology Laboratory, EMBL, Heidelberg D-69117, Germany; Department of Cell Physiology and Metabolism, University of Geneva, Genève 4 1211, Switzerland;* orcid.org/0000-0002-7677-8252

Anne-Claude Gavin − *Department of Cell Physiology and Metabolism, University of Geneva, Genève 4 1211, Switzerland*

Complete contact information is available at: https://pubs.acs.org/10.1021/acs.jpcb.4c02398

Author Contributions

M.M., N.R., and A.-C.G. performed conceptualization, methodologies, and supervision. M.M., P.G., R.T., A.C., and K.T. performed acquisition and analysis of data. M.M. performed visualization and writing of the original draft. M.M., P.G., K.T., N.R., and A.-C.G. reviewed and edited the manuscript. All authors discussed the results and participated in interpreting the results.

https://doi.org/10.1021/acs.jpcb.4c02398
J. Phys. Chem. B 2024, 128, 6338−6351

Funding

M.M. and N.R. acknowledge funding from the Research Council of Norway (Norges Forskningsråd, grant nos. 288008 and 335772). Computational resources were provided by NRIS/Sigma2 (no. nn4700k). A.-C.G. acknowledges financial support from the Louis-Jeantet Foundation. K.T. acknowledges financial support from the EU Marie Skłodowska-Curie Actions project 843407, LipTransProMet.

Notes

The authors declare no competing financial interest.

■ ACKNOWLEDGMENTS

We are grateful to members and former members of ACG's group at the Department of Cell Physiology and Metabolism, University of Geneva for continuous discussions and support.

■ REFERENCES

(1) van Meer, G.; Voelker, D. R.; Feigenson, G. W. Membrane Lipids: Where They Are and How They Behave. *Nat. Rev. Mol. Cell Biol.* **2008**, *9*, 112−124.
(2) Kumagai, K.; Hanada, K. Structure, Functions and Regulation of CERT, a Lipid-transfer Protein for the Delivery of Ceramide at the ER−Golgi Membrane Contact Sites. *FEBS Lett.* **2019**, *593*, 2366−2377.
(3) Hanada, K. Lipid Transfer Proteins Rectify Inter-Organelle Flux and Accurately Deliver Lipids at Membrane Contact Sites. *J. Lipid Res.* **2018**, *59*, 1341−1366.
(4) Sugiki, T.; Takeuchi, K.; Yamaji, T.; Takano, T.; Tokunaga, Y.; Kumagai, K.; Hanada, K.; Takahashi, H.; Shimada, I. Structural Basis for the Golgi Association by the Pleckstrin Homology Domain of the Ceramide Trafficking Protein (CERT). *J. Biol. Chem.* **2012**, *287*, 33706−33718.
(5) Kudo, N.; Kumagai, K.; Tomishige, N.; Yamaji, T.; Wakatsuki, S.; Nishijima, M.; Hanada, K.; Kato, R. Structural Basis for Specific Lipid Recognition by CERT Responsible for Nonvesicular Trafficking of Ceramide. *Proc. Natl. Acad. Sci. U. S. A.* **2008**, *105*, 488−493.
(6) Prashek, J.; Bouyain, S.; Fu, M.; Li, Y.; Berkes, D.; Yao, X. Interaction between the PH and START Domains of Ceramide Transfer Protein Competes with Phosphatidylinositol 4-Phosphate Binding by the PH Domain. *J. Biol. Chem.* **2017**, *292*, 14217−14228.
(7) Hanada, K.; Kumagai, K.; Yasuda, S.; Miura, Y.; Kawano, M.; Fukasawa, M.; Nishijima, M. Molecular Machinery for Non-Vesicular Trafficking of Ceramide. *Nature* **2003**, *426*, 803−809.
(8) Chiapparino, A.; Maeda, K.; Turei, D.; Saez-Rodriguez, J.; Gavin, A.-C. The Orchestra of Lipid-Transfer Proteins at the Crossroads between Metabolism and Signaling. *Prog. Lipid Res.* **2016**, *61*, 30−39.
(9) Wong, L. H.; Gatta, A. T.; Levine, T. P. Lipid Transfer Proteins: The Lipid Commute via Shuttles, Bridges and Tubes. *Nat. Rev. Mol. Cell Biol.* **2019**, *20*, 85−101.
(10) Schouten, A. Structure of Apo-Phosphatidylinositol Transfer Protein Alpha Provides Insight into Membrane Association. *EMBO J.* **2002**, *21*, 2117−2121.
(11) Grabon, A.; Orłowski, A.; Tripathi, A.; Vuorio, J.; Javanainen, M.; Róg, T.; Lönnfors, M.; McDermott, M. I.; Siebert, G.; Somerharju, P.; et al. Dynamics and Energetics of the Mammalian Phosphatidylinositol Transfer Protein Phospholipid Exchange Cycle. *J. Biol. Chem.* **2017**, *292*, 14438−14455.
(12) Miliara, X.; Garnett, J. A.; Tatsuta, T.; Abid Ali, F.; Baldie, H.; Pérez-Dorado, I.; Simpson, P.; Yague, E.; Langer, T.; Matthews, S. Structural Insight into the TRIAP 1/ PRELI -like Domain Family of Mitochondrial Phospholipid Transfer Complexes. *EMBO Rep.* **2015**, *16*, 824−835.
(13) Miliara, X.; Tatsuta, T.; Berry, J.-L.; Rouse, S. L.; Solak, K.; Chorev, D. S.; Wu, D.; Robinson, C. V.; Matthews, S.; Langer, T. Structural Determinants of Lipid Specificity within Ups/PRELI Lipid Transfer Proteins. *Nat. Commun.* **2019**, *10*, 1130.
(14) Watanabe, Y.; Tamura, Y.; Kawano, S.; Endo, T. Structural and Mechanistic Insights into Phospholipid Transfer by Ups1−Mdm35 in Mitochondria. *Nat. Commun.* **2015**, *6*, 7922.
(15) Kudo, N.; Kumagai, K.; Matsubara, R.; Kobayashi, S.; Hanada, K.; Wakatsuki, S.; Kato, R. Crystal Structures of the CERT START Domain with Inhibitors Provide Insights into the Mechanism of Ceramide Transfer. *J. Mol. Biol.* **2010**, *396*, 245−251.
(16) Mizuike, A.; Sakai, S.; Katoh, K.; Yamaji, T.; Hanada, K. The C10orf76−PI4KB Axis Orchestrates CERT-Mediated Ceramide Trafficking to the Distal Golgi. *J. Cell Biol.* **2023**, *222*, No. e202111069.
(17) Mouchlis, V. D.; Bucher, D.; McCammon, J. A.; Dennis, E. A. Membranes Serve as Allosteric Activators of Phospholipase A2, Enabling It to Extract, Bind, and Hydrolyze Phospholipid Substrates. *Proc. Natl. Acad. Sci. U. S. A.* **2015**, *112*, E516−E525.
(18) Yamamoto, E.; Akimoto, T.; Kalli, A. C.; Yasuoka, K.; Sansom, M. S. P. Dynamic Interactions between a Membrane Binding Protein and Lipids Induce Fluctuating Diffusivity. *Sci. Adv.* **2017**, *3*, No. e1601871.
(19) Yamamoto, E.; Domański, J.; Naughton, F. B.; Best, R. B.; Kalli, A. C.; Stansfeld, P. J.; Sansom, M. S. P. Multiple Lipid Binding Sites Determine the Affinity of PH Domains for Phosphoinositide-Containing Membranes. *Sci. Adv.* **2020**, *6*, No. eaay5736.
(20) Moqadam, M.; Tubiana, T.; Moutoussamy, E. E.; Reuter, N. Membrane Models for Molecular Simulations of Peripheral Membrane Proteins. *Adv. Phys. X* **2021**, *6*, 1932589.
(21) Le Huray, K. I. P.; Wang, H.; Sobott, F.; Kalli, A. C. Systematic Simulation of the Interactions of Pleckstrin Homology Domains with Membranes. *Sci. Adv.* **2022**, *8*, No. eabn6992.
(22) Larsen, A. H.; John, L. H.; Sansom, M. S. P.; Corey, R. A. Specific Interactions of Peripheral Membrane Proteins with Lipids: What Can Molecular Simulations Show Us? *Biosci. Rep.* **2022**, *42*, BSR20211406.
(23) Zhang, Y.; Soubias, O.; Pant, S.; Heinrich, F.; Vogel, A.; Li, J.; Li, Y.; Clifton, L. A.; Daum, S.; Bacia, K.; et al. Myr-Arf1 Conformational Flexibility at the Membrane Surface Sheds Light on the Interactions with ArfGAP ASAP1. *Nat. Commun.* **2023**, *14*, 7570.
(24) Lu, J.; Chan, C.; Yu, L.; Fan, J.; Sun, F.; Zhai, Y. Molecular Mechanism of Mitochondrial Phosphatidate Transfer by Ups1. *Commun. Biol.* **2020**, *3*, 468.
(25) Zhang, X.; Xie, H.; Iaea, D.; Khelashvili, G.; Weinstein, H.; Maxfield, F. R. Phosphatidylinositol Phosphates Modulate Interactions between the StarD4 Sterol Trafficking Protein and Lipid Membranes. *J. Biol. Chem.* **2022**, *298*, No. 102058.
(26) Talandashti, R.; Van Ek, L.; Gehin, C.; Xue, D.; Moqadam, M.; Gavin, A.-C.; Reuter, N. Membrane Specificity of the Human Cholesterol Transfer Protein STARD4. *J. Mol. Biol.* **2024**, *436*, No. 168572.
(27) Srinivasan, S.; Di Luca, A.; Peter, A. T. J.; Gehin, C.; Lone, M. A.; Hornemann, T.; D'Angelo, G.; Vanni, S. Conformational Dynamics of Lipid Transfer Domains Provide a General Framework to Decode Their Functional Mechanism. *bioxRiv*, 2023.
(28) Mouchlis, V. D.; Chen, Y.; McCammon, J. A.; Dennis, E. A. Membrane Allostery and Unique Hydrophobic Sites Promote Enzyme Substrate Specificity. *J. Am. Chem. Soc.* **2018**, *140*, 3285−3291.
(29) Mouchlis, V. D.; Hayashi, D.; Vasquez, A. M.; Cao, J.; McCammon, J. A.; Dennis, E. A. Lipoprotein-Associated Phospholipase A_2: A Paradigm for Allosteric Regulation by Membranes. *Proc. Natl. Acad. Sci. U. S. A.* **2022**, *119*, No. e2102953118.
(30) Berman, H. M. The Protein Data Bank. *Nucleic Acids Res.* **2000**, *28*, 235−242.
(31) Jo, S.; Kim, T.; Iyer, V. G.; Im, W. CHARMM-GUI: A Web-Based Graphical User Interface for CHARMM. *J. Comput. Chem.* **2008**, *29*, 1859−1865.
(32) Jorgensen, W. L.; Chandrasekhar, J.; Madura, J. D.; Impey, R. W.; Klein, M. L. Comparison of Simple Potential Functions for Simulating Liquid Water. *J. Chem. Phys.* **1983**, *79*, 926−935.

https://doi.org/10.1021/acs.jpcb.4c02398
J. Phys. Chem. B 2024, 128, 6338−6351

(33) Lomize, M. A.; Pogozheva, I. D.; Joo, H.; Mosberg, H. I.; Lomize, A. L. OPM Database and PPM Web Server: Resources for Positioning of Proteins in Membranes. *Nucleic Acids Res.* **2012**, *40*, D370−D376.
(34) Lee, J.; Cheng, X.; Swails, J. M.; Yeom, M. S.; Eastman, P. K.; Lemkul, J. A.; Wei, S.; Buckner, J.; Jeong, J. C.; Qi, Y.; et al. CHARMM-GUI Input Generator for NAMD, GROMACS, AMBER, OpenMM, and CHARMM/OpenMM Simulations Using the CHARMM36 Additive Force Field. *J. Chem. Theory Comput.* **2016**, *12*, 405−413.
(35) Phillips, J. C.; Braun, R.; Wang, W.; Gumbart, J.; Tajkhorshid, E.; Villa, E.; Chipot, C.; Skeel, R. D.; Kalé, L.; Schulten, K. Scalable Molecular Dynamics with NAMD. *J. Comput. Chem.* **2005**, *26*, 1781−1802.
(36) Klauda, J. B.; Venable, R. M.; Freites, J. A.; O'Connor, J. W.; Tobias, D. J.; Mondragon-Ramirez, C.; Vorobyov, I.; MacKerell, A. D.; Pastor, R. W. Update of the CHARMM All-Atom Additive Force Field for Lipids: Validation on Six Lipid Types. *J. Phys. Chem. B* **2010**, *114*, 7830−7843.
(37) Venable, R. M.; Sodt, A. J.; Rogaski, B.; Rui, H.; Hatcher, E.; MacKerell, A. D.; Pastor, R. W.; Klauda, J. B. CHARMM All-Atom Additive Force Field for Sphingomyelin: Elucidation of Hydrogen Bonding and of Positive Curvature. *Biophys. J.* **2014**, *107*, 134−145.
(38) Best, R. B.; Zhu, X.; Shim, J.; Lopes, P. E. M.; Mittal, J.; Feig, M.; MacKerell, A. D., Jr. Optimization of the Additive CHARMM All-Atom Protein Force Field Targeting Improved Sampling of the Backbone ϕ, ψ and Side-Chain X1 and X2 Dihedral Angles. *J. Chem. Theory Comput.* **2012**, *8*, 3257−3273.
(39) Khan, H. M.; MacKerell, A. D.; Reuter, N. Cation-π Interactions between Methylated Ammonium Groups and Tryptophan in the CHARMM36 Additive Force Field. *J. Chem. Theory Comput.* **2019**, *15*, 7−12.
(40) Khan, H. M.; Grauffel, C.; Broer, R.; MacKerell, A. D.; Havenith, R. W. A.; Reuter, N. Improving the Force Field Description of Tyrosine-Choline Cation-π Interactions: QM Investigation of Phenol-N$(Me)_4^+$ Interactions. *J. Chem. Theory Comput.* **2016**, *12*, 5585−5595.
(41) Jo, S.; Kim, T.; Im, W. Automated Builder and Database of Protein/Membrane Complexes for Molecular Dynamics Simulations. *PLoS One* **2007**, *2*, No. e880.
(42) Andersen, H. C. Rattle: A "Velocity" Version of the Shake Algorithm for Molecular Dynamics Calculations. *J. Comput. Phys.* **1983**, *52*, 24−34.
(43) Essmann, U.; Perera, L.; Berkowitz, M. L.; Darden, T.; Lee, H.; Pedersen, L. G. A Smooth Particle Mesh Ewald Method. *J. Chem. Phys.* **1995**, *103*, 8577−8593.
(44) Jo, S.; Cheng, X.; Islam, S. M.; Huang, L.; Rui, H.; Zhu, A.; Lee, H. S.; Qi, Y.; Han, W.; Vanommeslaeghe, K.; et al. Chapter Eight - CHARMM-GUI PDB Manipulator for Advanced Modeling and Simulations of Proteins Containing Nonstandard Residues. *Adv. Protein Chem. Struct. Biol.* **2014**, 235−265.
(45) Wu, E. L.; Cheng, X.; Jo, S.; Rui, H.; Song, K. C.; Dávila-Contreras, E. M.; Qi, Y.; Lee, J.; Monje-Galvan, V.; Venable, R. M.; et al. CHARMM-GUI *Membrane Builder* toward Realistic Biological Membrane Simulations. *J. Comput. Chem.* **2014**, *35*, 1997−2004.
(46) Humphrey, W.; Dalke, A.; Schulten, K. VMD: Visual molecular dynamics. *J. Mol. Graphics* **1996**, *14*, 33−38.
(47) Baker, N. A.; Sept, D.; Joseph, S.; Holst, M. J.; McCammon, J. A. Electrostatics of Nanosystems: Application to Microtubules and the Ribosome. *Proc. Natl. Acad. Sci. U. S. A.* **2001**, *98*, 10037−10041.
(48) *The PyMOL Molecular Graphics System*, Version 1.8; Schrödinger, LLC., 2015.
(49) Abraham, M. J.; Murtola, T.; Schulz, R.; Páll, S.; Smith, J. C.; Hess, B.; Lindahl, E. GROMACS: High Performance Molecular Simulations through Multi-Level Parallelism from Laptops to Supercomputers. *SoftwareX* **2015**, *1*−*2*, 19−25.
(50) Guixà-González, R.; Rodriguez-Espigares, I.; Ramírez-Anguita, J. M.; Carrió-Gaspar, P.; Martinez-Seara, H.; Giorgino, T.; Selent, J. MEMBPLUGIN: Studying Membrane Complexity in VMD. *Bioinformatics* **2014**, *30*, 1478−1480.
(51) Michaud-Agrawal, N.; Denning, E. J.; Woolf, T. B.; Beckstein, O. MDAnalysis: A Toolkit for the Analysis of Molecular Dynamics Simulations. *J. Comput. Chem.* **2011**, *32*, 2319−2327.
(52) Gowers, R.; Linke, M.; Barnoud, J.; Reddy, T.; Melo, M.; Seyler, S.; Domański, J.; Dotson, D.; Buchoux, S.; Kenney, I.et al.MDAnalysis: A Python Package for the Rapid Analysis of Molecular Dynamics Simulations. *Proceedings of the Python in Science Conference* SciPy: Austin Texas **2016**, 98 105 DOI: .
(53) Hayes, R. L.; Vilseck, J. Z.; Brooks, C. L. Approaching Protein Design with Multisite λ Dynamics: Accurate and Scalable Mutational Folding Free Energies in T4 Lysozyme. *Protein Sci.* **2018**, *27*, 1910−1922.
(54) Hayes, R. L.; Brooks, C. L. A Strategy for Proline and Glycine Mutations to Proteins with Alchemical Free Energy Calculations. *J. Comput. Chem.* **2021**, *42*, 1088−1094.
(55) Brooks, B. R.; Brooks, C. L.; Mackerell, A. D.; Nilsson, L.; Petrella, R. J.; Roux, B.; Won, Y.; Archontis, G.; Bartels, C.; Boresch, S.; et al. CHARMM: The Biomolecular Simulation Program. *J. Comput. Chem.* **2009**, *30*, 1545−1614.
(56) Hynninen, A.; Crowley, M. F. New Faster CHARMM Molecular Dynamics Engine. *J. Comput. Chem.* **2014**, *35*, 406−413.
(57) Hayes, R. L.; Buckner, J.; Brooks, C. L. BLaDE: A Basic Lambda Dynamics Engine for GPU-Accelerated Molecular Dynamics Free Energy Calculations. *J. Chem. Theory Comput.* **2021**, *17*, 6799−6807.
(58) Zambrano, F.; Fleischer, S.; Fleischer, B. Lipid Composition of the Golgi Apparatus of Rat Kidney and Liver in Comparison with Other Subcellular Organelles. *Biochim. Biophys. Acta, Lipids Lipid Metab.* **1975**, *380*, 357−369.
(59) Thomas, A. Lipids: Defining the Shape of Things to Come. *Nat. Cell Biol.* **1999**, *1*, E192−E192.
(60) Peeters, B. W. A.; Piët, A. C. A.; Fornerod, M. Generating Membrane Curvature at the Nuclear Pore: A Lipid Point of View. *Cells* **2022**, *11*, 469.
(61) Buckley, J. T. Cone-Shaped Lipids Increase the Susceptibility of Phospholipids in Bilayers to the Action of Phospholipases. *Can. J. Biochem. Cell Biol.* **1985**, *63*, 263−267.
(62) Grauffel, C.; Yang, B.; He, T.; Roberts, M. F.; Gershenson, A.; Reuter, N. Cation−π Interactions As Lipid-Specific Anchors for Phosphatidylinositol-Specific Phospholipase C. *J. Am. Chem. Soc.* **2013**, *135*, 5740−5750.
(63) Waheed, Q.; Khan, H. M.; He, T.; Roberts, M.; Gershenson, A.; Reuter, N. Interfacial Aromatics Mediating Cation−π Interactions with Choline-Containing Lipids Can Contribute as Much to Peripheral Protein Affinity for Membranes as Aromatics Inserted below the Phosphates. *J. Phys. Chem. Lett.* **2019**, *10*, 3972−3977.
(64) Fersht, A. R.; Shi, J.-P.; Knill-Jones, J.; Lowe, D. M.; Wilkinson, A. J.; Blow, D. M.; Brick, P.; Carter, P.; Waye, M. M. Y.; Winter, G. Hydrogen Bonding and Biological Specificity Analysed by Protein Engineering. *Nature* **1985**, *314*, 235−238.
(65) Williams, D. H.; Searle, M. S.; Mackay, J. P.; Gerhard, U.; Maplestone, R. A. Toward an Estimation of Binding Constants in Aqueous Solution: Studies of Associations of Vancomycin Group Antibiotics. *Proc. Natl. Acad. Sci. U. S. A.* **1993**, *90*, 1172−1178.
(66) Titeca, K.; Chiapparino, A.; Türei, D.; Zukowska, J.; Van Ek, L.; Moqadam, M.; Triana, S.; Nielsen, I. Ø.; Foged, M. M.; Gehin, C.et al.A System-Wide Analysis of Lipid Transfer Proteins Delineates Lipid Mobility in Human Cells. *bioRxiv*, **2023**.
(67) Kawano, M.; Kumagai, K.; Nishijima, M.; Hanada, K. Efficient Trafficking of Ceramide from the Endoplasmic Reticulum to the Golgi Apparatus Requires a VAMP-Associated Protein-Interacting FFAT Motif of CERT. *J. Biol. Chem.* **2006**, *281*, 30279−30288.
(68) Yee, S. M.; Gillams, R. J.; McLain, S. E.; Lorenz, C. D. Effects of Lipid Heterogeneity on Model Human Brain Lipid Membranes. *Soft Matter* **2021**, *17*, 126−135.
(69) Gao, Y.-G.; McDonald, J.; Malinina, L.; Patel, D. J.; Brown, R. E. Ceramide-1-Phosphate Transfer Protein Promotes Sphingolipid

https://doi.org/10.1021/acs.jpcb.4c02398
J. Phys. Chem. B 2024, 128, 6338−6351

Reorientation Needed for Binding during Membrane Interaction. *J. Lipid Res.* **2022**, *63*, No. 100151.
(70) Rogers, J. R.; Geissler, P. L. Ceramide-1-Phosphate Transfer Protein Enhances Lipid Transport by Disrupting Hydrophobic Lipid−Membrane Contacts. *PLOS Comput. Biol.* **2023**, *19*, No. e1010992.
(71) Huang, J. Chapter 12 Model Membrane Thermodynamics and Lateral Distribution of Cholesterol: From Experimental Data to Monte Carlo Simulation. *Methods Enzymol.* **2009**, 329−364.
(72) Alwarawrah, M.; Dai, J.; Huang, J. Modification of Lipid Bilayer Structure by Diacylglycerol: A Comparative Study of Diacylglycerol and Cholesterol. *J. Chem. Theory Comput.* **2012**, *8*, 749−758.
(73) Kwolek, U.; Kulig, W.; Wydro, P.; Nowakowska, M.; Róg, T.; Kepczynski, M. Effect of Phosphatidic Acid on Biomembrane: Experimental and Molecular Dynamics Simulations Study. *J. Phys. Chem. B* **2015**, *119*, 10042−10051.
(74) Alwarawrah, M.; Hussain, F.; Huang, J. Alteration of Lipid Membrane Structure and Dynamics by Diacylglycerols with Unsaturated Chains. *Biochim. Biophys. Acta, Biomembr.* **2016**, *1858*, 253−263.
(75) Rogers, J. R.; Espinoza Garcia, G.; Geissler, P. L. Membrane Hydrophobicity Determines the Activation Free Energy of Passive Lipid Transport. *Biophys. J.* **2021**, *120*, 3718−3731.
(76) Sha, B.; Luo, M. PI Transfer Protein: The Specific Recognition of Phospholipids and Its Functions. *Biochim. Biophys. Acta, Mol. Cell Biol. Lipids* **1999**, *1441*, 268−277.
(77) Wirtz, K. W. A. Phospholipid Transfer Proteins in Perspective. *FEBS Lett.* **2006**, *580*, 5436−5441.
(78) Brown, R. E.; Mattjus, P. Glycolipid Transfer Proteins. *Biochim. Biophys. Acta, Mol. Cell Biol. Lipids* **2007**, *1771*, 746−760.
(79) Jiang, X.-C.; Zhou, H.-W. Plasma Lipid Transfer Proteins. *Curr. Opin. Lipidol.* **2006**, *17*, 302−308.
(80) Tuuf, J.; Kjellberg, M. A.; Molotkovsky, J. G.; Hanada, K.; Mattjus, P. The Intermembrane Ceramide Transport Catalyzed by CERT Is Sensitive to the Lipid Environment. *Biochim. Biophys. Acta, Biomembr.* **2011**, *1808*, 229−235.
(81) Hanada, K. Co-Evolution of Sphingomyelin and the Ceramide Transport Protein CERT. *Biochim. Biophys. Acta, Mol. Cell Biol. Lipids* **2014**, *1841*, 704−719.
(82) Schaaf, G.; Ortlund, E. A.; Tyeryar, K. R.; Mousley, C. J.; Ile, K. E.; Garrett, T. A.; Ren, J.; Woolls, M. J.; Raetz, C. R. H.; Redinbo, M. R.; et al. Functional Anatomy of Phospholipid Binding and Regulation of Phosphoinositide Homeostasis by Proteins of the Sec14 Superfamily. *Mol. Cell* **2008**, *29*, 191−206.

https://doi.org/10.1021/acs.jpcb.4c02398
J. Phys. Chem. B 2024, 128, 6338−6351